K. Matsui[1], A. Ogawa[1], J. Kikuma[2], M. Tsunashima[2], T. Ishikawa[2], S. Matsuno[2]

[1]Construction Materials Laboratory, Asahi-KASEI Construction Materials Corporation, Japan

[2]Analysis and Simulation Center, Asahi-KASEI Corporation, Japan

Influence of addition of Al compound and gypsum on tobermorite formation in autoclaved aerated concrete studied by *in situ* X-ray diffraction

ABSTRACT: The hydrothermal formation of tobermorite during the processing of autoclaved aerated concrete was investigated by *in situ* XRD analysis. The XRD measurement is carried out using high-energy X-rays from a synchrotron radiation source. The effects of Al and gypsum addition on tobermorite formation were studied. Acceleration of tobermorite formation by Al and gypsum addition was clearly observed. The tobermorite formation mechanisms were discussed in these systems.

KEY WORDS: AAC, *in situ* XRD, tobermorite, C-S-H, katoite, gypsum

1. Introduction

Since both the quantity and quality of tobermorite formed in autoclaved aerated concrete (AAC) significantly affect its mechanical properties (Mitsuda et al. 1992), understanding the mechanism of tobermorite formation during hydrothermal treatment (i.e., the autoclaving process) is important in AAC production. The synthesis of tobermorite under hydrothermal conditions has been extensively studied for various starting materials including several types of silica sources and various additives. It has been revealed that Al compounds and gypsum significantly affect the tobermorite formation process (Larosa-Thompson et al. 1996, Sakiyama et al. 2000). However, this process is more complex in industrial AAC production because of various impurities in raw materials. Therefore, the formation mechanism of tobermorite is not thoroughly understood.

We have developed a relatively large autoclave cell for *in situ* transmission X-ray diffraction, which has sufficient space for the sample and the water reservoir. The formation process of tobermorite from cement-based starting materials has been successfully observed (Kikuma et al. 2009, 2010). In the present study, we applied this method to the AAC autoclave process, and the effects of adding Al compounds and gypsum to the tobermorite formation reaction in AAC production were investigated.

2. Experimental

2.1. Materials and sample preparation

The compositions of the starting materials are shown in Table 1. Two types of crushed quartz were used as silica sources: (A) quartz rock (purity >96.9%) and (B) quartz sand (purity >96.8%). High early strength Portland cement (HPC) was purchased from Ube-Mitsubishi, Ube, Japan. γ-Al_2O_3, quicklime and gypsum were research grade. The starting mixtures were fully mixed in the presence of water at 50°C. The water-to-solid ratio was 0.75 by weight. For each run, the slurry mixture was poured into a plastic beaker and kept at 60°C for more than 12 h for the cement in the mixture to become hydrated. The hydrated mixture was then cooled, and cut into a specimen with dimensions of 6 mm ÷ 18 mm and thickness of 3.0 mm, immediately before the *in situ* measurement was conducted. In this study we did not use a foaming agent (e.g., Al metal powder), to avoid nonuniformity of X-ray transmission in the samples.

Table 1

COMPOSITION OF THE STARTING MATERIALS

Experiments		Al addition		gypsum addition	
Samples		A (without Al)	B (with Al)	C (without gypsum)	D (with gypsum)
Quartz (type)	(mass %)	54.4 (quartz A)	51.5 (quartz A)	55.7 (quartz B)	53.5 (quartz B)
Quicklime	(mass %)	4.7	4.9	5.4	5.1
HPC	(mass %)	38.9	38.9	38.9	37.4
Gypsum	(mass %)	2.0	2.0	0	4.0
γ-Al_2O_3	(mass %)	0	2.7	0	0
Ca/(Si+Al)	(mole ratio)	0.51	0.51	0.51	0.51
Al/(Si+Al)	(mole ratio)	0.037	0.088	0.037	0.037

2.2. *In situ XRD measurement*

XRD measurements were carried out at the BL19B2 beamline of SPring-8 in Japan using an X-ray energy of 30 keV. The X-ray energy was selected so that the transmittance of the X-ray

through the sample would be around 50%. The temperature of the autoclave cell was controlled by a copper heater block surrounded by a thermal insulator. First, the temperature was raised to 100°C at a rate of 2°C/min. The temperature was held at 100°C for 15 min. During this period, the cell was evacuated for a few seconds, and about 95% of the air was removed from the cell. After the steam pressure was built up again at 100°C, the first XRD measurement was conducted. After 15 min at 100°C, the temperature was raised again to 190°C at a rate of 1°C/min, and then held at 190°C for 12 h. During this process, the XRD measurements were conducted using a photon-counting pixel array detector, PILATUS 100 K (DECTRIS, Baden, Switzerland). The measurement interval was 4.25 min. During the exposure time, the cell, together with the heater block, was oscillated in the vertical direction by 3.0 mm at a rate of 0.6 mm/s to average over a larger area of the sample.

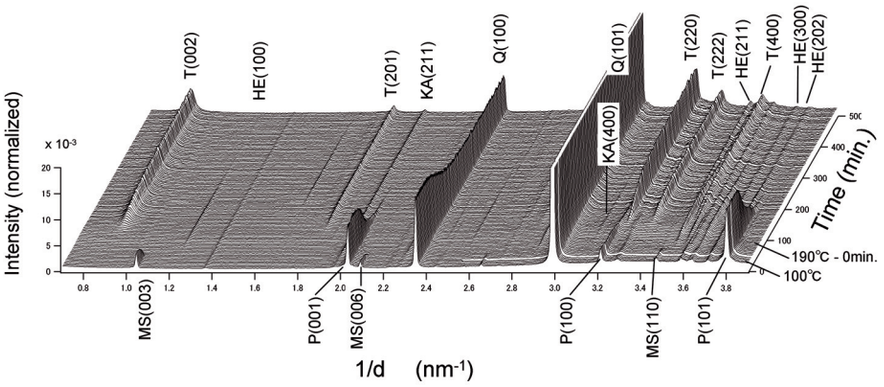

Fig. 1. Stack of time-resolved XRD patterns for sample without Al addition. Temperature was raised from 100 to 190°C and held at 190°C. T, tobermorite; P, portlandite; Q, quartz; MS, monosulfate; KA, katoite; HE, hydroxylellestadite.

2.3. Analysis of non-crystalline phase

In the present *in situ* experiment, we were able to observe the intensity change of an amorphous halo at around 3.4 nm^{-1}, where the halo of non-crystalline C-S-H is observed. Non-crystalline C-S-H is formed by the hydration of cement and is well-known as a major precursor to tobermorite formation. The integrated intensity from 3.427 to 3.434 nm^{-1} was regarded as the C-S-H intensity in our previous studies (Kikuma et al. 2009, 2010). In the present study this method was used to estimate the quantity of C-S-H.

3. Results and discussion

3.1. Phase evolution in experiments on Al addition

Figure 1 shows the time-resolved XRD data set for the sample without Al addition. Several constituents involved in the reaction are clearly observed. The time course of normalized peak intensity for each major constituent is plotted in Fig. 2(a) and (b) for samples without and with Al addition, respectively. The sum of the (211) and (002) peaks intensities for hydroxylellestadite (HE: $Ca_{10}(SiO_4)_3(SO_4)_3(OH)_2$), and the sum of the (211) and (220) peaks intensities for katoite (KA: $Ca_3Al_2(SiO_4)_{3-x}(OH)_{4x}$; x = 1.5 to 3.0), a type of hydrogarnet, are plotted to obtain larger peak integrals and better statistics. For tobermorite, the (002) and (220) peaks are separately plotted. All data are normalized on the basis of XRD measurements of the same sample in our laboratory after *in situ* XRD.

In these two experiments, monosulfate (MS: $Ca_4Al_2O_6(SO_4)\cdot 14H_2O$) and portlandite (P: $Ca(OH)_2$) were observed at the beginning of the autoclave process, and their intensities decreased as the reactions proceeded. Finally both phases completely disappeared. Quartz initially decreased slowly, and the decreasing rate became slightly faster in the middle stage and then became slower again toward the end. As intermediate phases, KA and HE were observed in the middle of the reactions. In the later stage HE decreased and disappeared, whereas KA decreased slowly and partly remained. Tobermorite began to be observed after the temperature reached 190°C, at which the intensity of C-S-H reached maximum. Then, tobermorite formation increased toward the end of the autoclave process. Anhydrite (A: $CaSO_4$) began to be observed when HE reached maximum, and then increased gradually until the end. This suggests that SO_4^{2-} ions released from HE are involved in anhydrite formation.

3.2. Tobermorite formation via C-S-H and KA

As shown in Fig. 2, Al addition accelerated crystallization of tobermorite, especially along the c-axis (002) direction, On the other hand, C-S-H and KA exhibited unique behavior with Al addition. To clarify this point, the relation between C-S-H and tobermorite intensity is plotted in Fig. 3 and the relation between KA and tober-

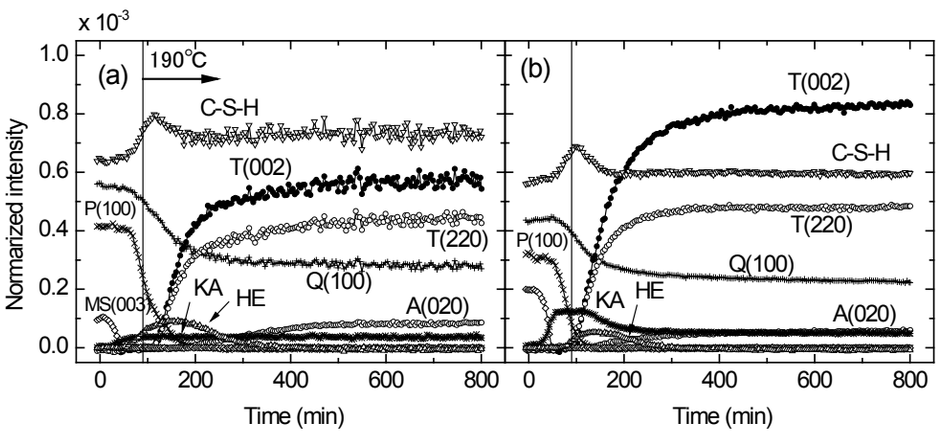

Fig. 2. Time course of normalized peak intensity for each major constituent during the autoclave process: (a) sample without Al addition and (b) sample with 5 mol % Al addition.

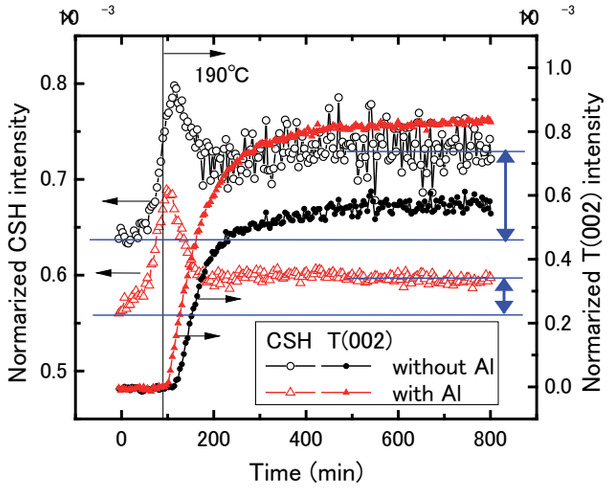

Fig. 3. Time courses of C-S-H and tobermorite (002) intensities for samples without Al addition and with 5 mol % Al addition.

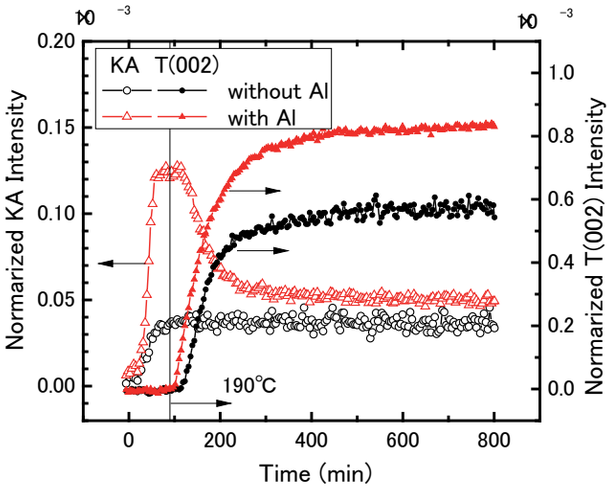

Fig. 4. Time courses of KA (katoite) and tobermorite (002) intensities for samples without Al addition and with 5 mol % Al addition.

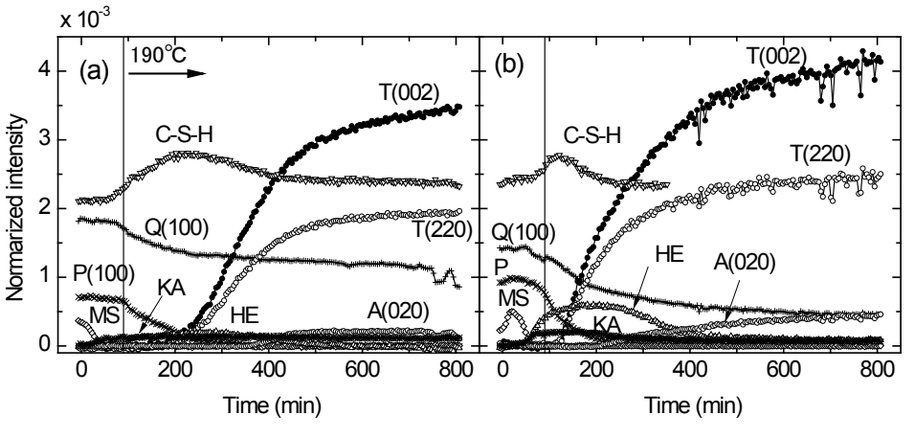

Fig. 5. Time course of peak intensity for each major constituent during the autoclave process: (a) sample and (b) sample with 4 wt % gypsum addition.

morite intensity is plotted in Fig. 4. It can be seen in both figures that after the temperature reached 190ºC, C-S-H and KA (with Al addition) decreased with increasing intensity of tobermorite. This suggests that there are at least two pathways to tobermorite formation, namely, the C-S-H route and the KA route. For the C-S-H behavior shown in Fig. 3, the amount of remaining C-S-H (length of vertical arrow) was decreased by Al addition. In other words, tobermorite formation via C-S-H was accelerated by Al addition. Consequently, the main route of tobermorite formation may shift from the C-S-H route to the KA route.

3.3. Phase evolution in experiments on gypsum addition

The time course of the relative peak intensity of each major constituent for samples without gypsum addition and with 4 wt % gypsum addition are plotted in Fig. 5(a) and (b), respectively. For both samples, the start of tobermorite formation corresponded to the maximum of the C-S-H intensity, and the tobermorite intensity increased with decreasing C-S-H intensity. It is reasonable to consider that the most of the tobermorite phase was formed via C-S-H phase in the same manner as in the experiments on Al addition. For the sample with gypsum addition, the tobermorite formation began earlier than that for the sample without gypsum addition. Further, the tobermorite formation rate became larger in the initial stage of the reaction. It was clearly observed that MS, HE, and anhydrite intensities became stronger due to the increased concentration of SO_4^{2-} ions from the gypsum (Fig. 5(b)). In this system, the timing of maximum HE intensity was identical to the starting point of anhydrite formation. Several studies have reported that HE decomposes into anhydrite and tobermorite under hydrothermal processing (Sakiyama et al. 2000). Our results are consistent with these studies. Therefore, tobermorite formation via HE is considered to be an important reaction route in addition to the KA and C-S-H routes mentioned above.

3.4. Kinetics of tobermorite formation

In situ XRD analysis is highly advantageous for studying hydrothermal reactions because of its high time resolution. We attempted to analyze the kinetics of the tobermorite formation reaction using the Avrami equation, which has been used to describe crystallization involving nucleation and growth (Avrami 1939):

$$\alpha = 1 - \exp[-k\,(t - t_0)^n]. \qquad (1)$$

Here, the parameter α is the degree of the reaction, k is the rate constant for the reaction, t is the reaction time, t_0 is the induction time, and n is a constant that indicates the reaction mechanism. The n value can be calculated from the slope of a plot of $-\ln[\ln(1-\alpha)]$ versus $\ln(t-t_0)$ (Hancock et al. 1972). In this study, α was calculated from the tobermorite (222) intensity and t_0 was defined as the starting point of tobermorite formation in Fig. 5(a) and (b). The plots of $-\ln[\ln(1-\alpha)]$ versus $\ln(t-t_0)$ had good linear correlation over α = 0.13−0.93 for both samples, yielding n values of 2.15 for the sample without gypsum addition

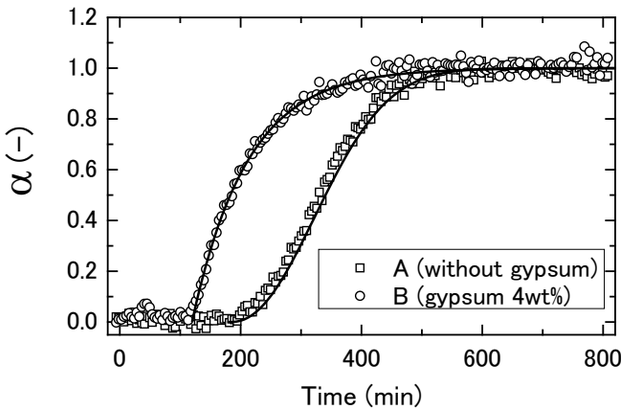

Fig. 6 Time dependence of the degree of reaction (α) calculated from the tobermorite (222) intensity and the theoretical curve from the Avrami model, for samples without gypsum addition and with 4 wt % gypsum addition.

and 1.00 for the sample with gypsum addition. Figure 6 shows time course of the degree of the reaction and the calculated theoretical curves using the *n* values.

The Avrami exponent *n* has been defined more exactly in terms of three additional constants (Brown et al. 1985):

$$n = (P/S) + Q. \quad (2)$$

Here, *P* is a dimensionality constant for the growth of product: *P* = 1 for one-dimensional growth (fibers, needles, etc.); *P* = 2 for two-dimensional growth (plates, sheets); and *P* = 3 for three-dimensional growth. *S* is related to the rate-limiting growth mechanism: *S* = 1 for interface- or phase boundary-controlled growth, or *S* = 2 for diffusion-controlled growth. *Q* is a constant that indicates the nucleation rate: *Q* = 1 for a constant nucleation rate, and *Q* = 0 for nucleation site saturation (zero nucleation rate). It is reasonable to assume that *P/S* in equation (2) is 1 in the present experiments; that is, *P* = 2 (plate growth) and *S* = 2 (diffusion-controlled process). Consequently, *Q* = 1.15 for the sample without gypsum and *Q* = 0 for the sample with gypsum addition. Therefore, all nucleation sites were saturated and tobermorite crystallized without further formation of nuclei in the system having high sulfate ion concentration. On the other hand, tobermorite crystallized with nucleation in the system having a lower sulfate ion concentration. The fact that the induction time was shorter and the initial formation rate was higher in the system with added gypsum supports this hypothesis. It is not clear how sulfate ions may affect the nucleation. Additional studies of this nucleation effect should be conducted.

4. Conclusion

With consideration of the effects of Al addition and gypsum addition, the hydrothermal formation reaction of tobermorite in the AAC process has been investigated by *in situ* X-ray diffraction. Both additives clearly accelerated tobermorite formation in the AAC process. As intermediate phases, non-crystalline calcium silicate hydrate (C-S-H), hydroxylellestadite (HE), and katoite (KA) were clearly observed. It was confirmed that there were reaction pathways to tobermorite formation via C-S-H, KA, and HE. In the experiment on gypsum addition, the Avrami model was well fitted over almost the entire reaction period, and different exponent coefficients were obtained for the two systems. These findings suggested on the one hand that the reaction proceeded in parallel with nucleation in the system with lower sulfate ion concentration, and on the other hand that nucleation was completed before tobermorite appeared and it subsequently began to form and continued until the reaction's end in the system with higher sulfate ion concentration.

Acknowledgments

This study was performed with the approval of JASRI (Proposal Nos. 2008B1864, 2008B2031 and 2009B1788).

Bibliography

[1] Avrami M., 1939, Kinetics of phase change. I, J. Chem. Phys, **7**, 1103-1112

[2] Brown P.W., Pommersheim J., Frohnsdorff G., 1985, A kinetic model for the hydration of tricalcium silicate, Cem. Concr. Res., **15**, 35-41.

[3] Hancock J.D., Sharp J.H., 1972, Method of comparing solid-state kinetic data and its application to the decomposition of kaolinite, brucite, and $BaCO_3$, J. Am. Ceram. Soc., **55**, 74-77.

[4] Kikuma J., Tsunashima M., Ishikawa T., Matsuno S., Ogawa A., Matsui K., Sato M., 2009. Hydrothermal formation of tobermorite studied by in-situ X-ray diffraction under autoclave condition, J. Synchrotron Rad., **16**, 683-686.

[5] Kikuma J., Tsunashima M., Ishikawa T., Matsuno S., Ogawa A., Matsui K., Sato M., 2010. *In-situ* time-resolved X-ray diffraction of tobermorite formation process under autoclave condition, J. Am. Ceram. Soc., **93**, 2667-2674.

[6] Larosa-Thompson J.L., Grutzeck M.W., 1996. C-S-H, tobermorite, and coexisting phases in the system CaO-Al_2O_3-SiO_2-H_2O, World Cement, **27**, 69-74

[7] Mitsuda, T., Sasaki K., Ishida H., 1992. Phase evolution during autoclaving process of aerated concrete, J. Am. Ceram. Soc., **75**, 1858-1863.

[8] Sakiyama M., Oshio Y., Mitsuda T., 2000, Influence of gypsum on the hydrothermal reaction of lime-quartz system and on the strength of autoclaved calcium silicate product, J. Soc. Inorganic Mater. Jpn., **7**, 685-691.